Experimental Neurology 320 (2019) 113004

Contents lists available at ScienceDirect

Experimental Neurology

journal homepage: www.elsevier.com/locate/yexnr

Research paper

Neuroinflammation in the pathogenesis of axonal Charcot-Marie-Tooth disease caused by lack of GDAP1

Sara Fernandez-Lizarbe[a,1,2], Azahara Civera-Tregón[b,c,1], Lara Cantarero[b,c], Isabel Herrer[a,3], Paula Juarez[a,4], Janet Hoenicka[b,d], Francesc Palau[b,c,e,f,g,*]

[a] Centro de Investigación Príncipe Felipe, Valencia, Spain
[b] Laboratory of Neurogenetics and Molecular Medicine – IPER, Institut de Recerca Sant Joan de Déu, Barcelona, Spain
[c] Centro de Investigación Biomédica en Red de Enfermedades Raras (CIBERER), Barcelona, Spain
[d] Centro de Investigación Biomédica en Red de Salud Mental (CIBESAM), Barcelona, Spain
[e] Department of Genetic and Molecular Medicine – IPER, Hospital Sant Joan de Déu, Barcelona, Spain
[f] Clinic Institute of Medicine and Dermatology (ICMiD), Hospital Clínic, Barcelona, Spain
[g] Division of Pediatrics, Faculty of Medicine and Health Sciences, University of Barcelona, Barcelona, Spain

ARTICLE INFO

Keywords:
Charcot-Marie-tooth disease
Axonopathy
GDAP1
Neuroinflammation
Gdap1 knockout mouse

ABSTRACT

Mutations in the *GDAP1* mitochondrial outer membrane gene cause Charcot-Marie-Tooth (CMT) neuropathy. Reduction or absence of GDAP1 has been associated with abnormal changes in the mitochondrial morphology and dynamics, oxidative stress and changes in calcium homeostasis. Neuroinflammation has been described in rodent models of genetic demyelinating CMT neuropathies but not in CMT primarily associated with axonopathy. Inflammatory processes have also been related to mitochondrial changes and oxidative stress in central neurodegenerative disorders. Here we investigated the presence of neuroinflammation in the axonal neuropathy of the *Gdap1*$^{-/-}$ mice. We showed by transcriptome profile of spinal cord and the *in vivo* detection of activated phagocytes that the absence of GDAP1 is associated with upregulation of inflammatory pathways. We observed reactive gliosis in spinal cord with increase of the astroglia markers GFAP and S100B, and the microglia marker IBA1. Additionally, we found significant increase of inflammatory mediators such as TNF-α and pERK, and C1qa and C1qb proteins of the complement system. Importantly, we observed an increased expression of CD206 and CD86 as M2 and M1 microglia and macrophage response markers, respectively, in *Gdap1*$^{-/-}$ mice. These inflammatory changes were also associated with abnormal molecular changes in synapses. In summary, we demonstrate that inflammation in spinal cord and sciatic nerve, but not in brain and cerebellum, is part of the pathophysiology of axonal *GDAP1*-related CMT.

1. Introduction

Charcot-Marie-Tooth (CMT) disease is the most common hereditary condition of the peripheral nervous system. CMT is a genetic heterogeneous disease, which involves both motor and sensory nerves and is characterized by distal muscle weakness and atrophy, leading to motor handicap, distal sensory loss and *pes cavus* with wide clinical expression severity (Rossor et al., 2016). Mutations in CMT-associated genes can be expressed as primary lesion of either myelin or axonalperipheral nerve, and pathogenic mechanisms involve a wide range of biological processes and pathways (Jerath et al., 2015). *GDAP1* (Ganglioside-induced differentiation-associated protein 1) gene mutations cause axonal CMT with both recessive (AR-CMT2K) (Cuesta et al., 2002) and dominant (CMT2K) inheritance (Claramunt et al., 2005), and recessive demyelinating CMT4A (Baxter et al., 2002). GDAP1 is located at the mitochondrial outer membrane (MOM) (Niemann et al., 2005; Pedrola et al., 2005) and at mitochondrial associated membranes (MAMs) (Pla-Martin et al., 2013). We have demonstrated that mutant GDAP1 cause defects in mitochondrial dynamics and calcium handling (Pla-Martin et al., 2013; Barneo-Munoz et al., 2015; Gonzalez-Sanchez et al., 2017).

* Corresponding author at: Hospital Sant Joan de Déu, Passeig Sant Joan de Déu 2, 08950 Esplugues de Llobregat, Barcelona, Spain.
E-mail address: fpalau@sjdhospitalbarcelona.org (F. Palau).
[1] These authors contributed equally.
[2] Cell Culture and Flow Cytometry Service, University of Valencia, Burjassot, Spain.
[3] Department of Education and Culture, Government of Aragon, Zaragoza, Spain.
[4] Agilent Technologies SL, Valencia, Spain.

https://doi.org/10.1016/j.expneurol.2019.113004
Received 1 September 2018; Received in revised form 17 June 2019; Accepted 28 June 2019
Available online 02 July 2019
0014-4886/

GDAP1 also participates in the defense against oxidative stress (Noack et al., 2011).

To date in CMT disease, the inflammatory process and activation of macrophages has been documented in animal models of demyelinating forms (Martini and Willison, 2016) but not in axonal forms. We have reported a *Gdap1* knockout mouse (*Gdap1*$^{-/-}$) that resembles the autosomal recessive axonal AR-CMT2K form of *GDAP1*-related CMT neuropathies. *Gdap1*$^{-/-}$ mice show a motor and sensory neuropathy with a reduction of compound muscle potential action (CMAP) amplitudes, motor nerve conduction velocities (MNCVs) (Barneo-Munoz et al., 2015). In addition, *Gdap1*-null mice show abnormal thermal and mechanical nociceptive sensitivities related to defects in the peripheral nervous system (Martínez-Valero, 2017). Therefore, *Gdap1* knockout mouse model offers the opportunity to investigate the role of neuroinflammation in axonal peripheral neuropathies in which the primary defect involves a gene that produces mitochondrial and metabolic alterations. It is known that abnormal mitochondria function generates oxidative stress causing inflammation responses that are relevant in the pathophysiology of neurological diseases (Di Filippo et al., 2010; Lopez-Armada et al., 2013). Here, we demonstrate that the absence of GDAP1 causes an inflammatory response in mice that involves the innate immune system and may accelerate the neurodegenerative process of CMT disease.

2. Material and methods

2.1. Animals

The *Gdap1* knockout (*Gdap1*$^{-/-}$) mice were previously generated and characterized in our laboratory (Barneo-Munoz et al., 2015). Gdap1 −/− and wild type (WT) mice at 12-month-old were sacrificed by gentle cervical dislocation and used as RNA, protein and tissue source. Expression of inflammatory cytokines and mediators were also investigated in 5-month-old mice. All the animals were kept under controlled temperature (23 °C) and humidity (60%) on a 12 h light/dark cycle with access of food and water *ad libitum*. Experimental procedures were performed following the European Union Council guidelines (2010/63/EU) and Spanish regulations (RD1201/2005), and were approved by the local Research and Ethics Committee of the Príncipe Felipe Research Center (CIPF).

2.2. Motor neuron primary cell culture

Primary cell cultures of motor neurons (MNs) were prepared from E13.5 mouse as described (Gingras et al., 2007) with some modifications (Barneo-Munoz et al., 2015). Ventral spinal cords were disaggregated enzymatically in glucose–HEPES (GHEBS) buffer solution (137 mM NaCl, 2.7 mM KCl, 22.2 mM glucose, 25 mM HEPES buffer pH 7.4, 20 IU/mL penicillin, 20 mg/mL streptomycin) containing 0.025% trypsin for 9 min at 37 °C, followed by mechanical dissociation. Cells were collected under a 4% bovine serum albumin (BSA) gradient. MNs were isolated by centrifugation (10 min at 520*g*) on a density gradient 11.5% OptiPrep (Sigma-Aldrich) in GHEBS buffer and platting in a complete medium: Neurobasal (Life technologies) supplemented with B27 (Life technologies), 2% horse serum, 1× glutamax (Life technologies), and a cocktail of recombinant neurotrofins: 1 ng/mL BDNF, 10 ng/mL GDNF, 10 ng/mL CNTF, and 10 ng/mL HGF (PreProtech) on poly-D-lysine/laminin-coated surfaces as described previously (Soler et al., 1998). MNs were grown in a 5% CO_2 incubator at 37 °C.

2.3. Transcriptome analysis

Total RNA was extracted from lumbar spinal cord dissected and snap frozen in liquid nitrogen using the Rneasy Mini Kit (Qiagenp/n 74,106). RNA was quantified by spectrometry (NanoDrop ND1000, NanoDrop Technologies) and quality was confirmed by RNA 6000 Nano Bioanalyzer (Agilent Technologies) assay. Total RNA was used to produce Cyanine 3-CTP-labeled cRNA using the Low Input Quick Amp Labelling Kit (One-Color, Agilent p/n 5190-2305) according to the manufacturer's instructions. Following 'One-Color Microarray-Based Gene Expression Analysis' protocol Version 6.7 (Agilent p/n G4140-90040), 600 ng of labeled cRNA was hybridized with the SurePrint G3 Mouse Gene Expression v2 Microarray, 8x60K (Agilent p/n G4852A-028005) containing 55,680 + probes. Arrays were scanned in an Agilent Microarray Scanner (Agilent G2565C) according to the manufacturer's protocol and data extracted using Agilent Feature Extraction Software 11.5.1.1 following the Agilent protocol GE1_1105_Oct12, grid template 028005_D_F_20140728 and the QC Metric Set GE1_QCMT_Oct12. To find differentially expressed genes and pathway enrichment analysis, normalized data were used for statistical analysis using *limma* moderated t-statistics ($p \leq 0.05$). Data were normalized by *Z*-Score and the heatmap visualized by R gplots. Data analysis was carried out in the Genomic Core Facility of the Principe Felipe Research Center.

2.4. In vivo imaging

Three wild type (WT) and three *Gdap1*$^{-/-}$ mice were anesthetized with 5% isoflurane and hair was removed. Mice received intraperitoneal Xenolight Rediject Inflammation Probe (Perkin Elmer) at a dose of 200 mg/kg which allows for *in vivo* assessment of myeloperoxidase activity of activated phagocytes. The bioluminescence was acquired using the IVIS bioluminescence/fluorescence optical imaging system at different time points after injection. Each image was acquired with 5-s exposure times using 750 nm excitation and 800 nm emission filter set. Regions of interest (ROIs) were manually drawn around the bodies of the mice to assess the relative signal intensity emitted. The optical signal was quantified using Living Image Software (Caliper Life Sciences) and photon flux was expressed as the average radiance in photon/s/cm^2/sr. Optical images were used for quantitative analysis of the total and maximum radiant efficiency within each ROI.

2.5. Measuring ROS production and mitochondrial superoxide

MNs were seeded in a 96-well plate in a density of 20,000 cells/well. MNs at 2 DIV were treated with 500 μM hydrogen peroxide for 10 min as a positive control. The ROS production were analyzed with carboxy-2′,7′- dichlorodihydrofluoresceinediacetate (DCFH-DA) as previously described (Qin et al., 2004). The production of mitochondrial superoxide was detected by MitoSOX Red reagent (Molecular Probes), following manufacture instructions. MNs were exposed to 20 μM DCFH-DA for 30 min or 5 μM Mitosox for 10 min at 37 °C in HCSS (120 mM NaCl, 0.8 mM MgCl2, 25 mM HEPES, 5.4 mM KCl, pH 7.4), 2.5 mM glucose, 2 mM Ca2+. Then, the medium was removed and the fluorescence was read immediately at the wavelengths of 485 nm for excitation and 530 nm for emission for the detection of DCF and 510 nm for excitation and 580 nm for emission of MitoSOX using a Victor-II spectrofluorimeter plate reader (Wallac).

2.6. Measuring cell viability

For neuronal viability analysis, MNs were seeded in 96 well coated plate and at 2 DIV treated or not with 10 μM camptotecine overnight as positive control. The next day, MNs were incubated during 30 min at 4 °C with 1 μM YO-PRO-1 (491/509 nm) and 1 μg/ml Hoechst 33342 (350/461 nm), followed by 2 μg/ml of propidium iodide (493/633 nm) during 10 min. This dual staining was used to differentiate between necrosis (propidium iodide positive labeled) and apoptosis (YO-PRO-1 positive labeled). Images were acquired and analyzed by using the In Cell Analyzer 2200 (GE Healthcare Life Science).

2.7. Western blotting

Total proteins were obtained from snap frozen in liquid nitrogen tissues (brain, cerebellum, spinal cord and sciatic nerves) using lysis buffer (50 mM Tris/HCl pH 7.4, 1.5 mM $MgCl_2$, 5 mM EDTA, 1% (*v*/v) Triton X100, 50 mM NaF, 1 mM Na_2VO_3, 1 mM DTT) containing a cocktail of protease inhibitor (Roche). Samples were centrifuged (15,000 *g*) at 4 °C for 30 min and the supernatant was collected. The protein concentration was determined with the Bradford reagent (Bio-Rad Protein Assay) using BSA as standard. Equal amounts of proteins (30 µg) of each sample were load onto SDS-polyacrylamide gels and transferred to a polyvinylidene fluoride membrane (EMD Millipore). Membranes were blocked with 5% dried milk or 5% BSA for phosphorylated proteins in TBS containing 0.1% Tween-20, and then incubated overnight at 4 °C using the following antibodies: α-pERK1/2 (1:100), α-ERK1/2 (1:100), α-pJNK (1:100), α-JNK (1:100), α-IRF3 (1:250) and α-TNF-α (1:300) from Santa Cruz Biotechnology; α-PSD95 (1/400) and α-SYNAPSIN-1 (1:300) from Abcam. After washing, blots were incubated with a goat α-rabbit peroxidase-conjugated IgG or goat α-mouse peroxidase-conjugated IgG (1:10,000; Abcam) during 1 h at room temperature (RT) and proteins were visualized using the ECL Prime chemiluminescent substrate (GE Healthcare Amersham). The bands intensity was measured through total area of the peaks using the AlphaImager2200 software (Alpha Innotech Corporation).

2.8. Quantitative real-time RT-PCR

Total RNA was isolated from tissues or MNs with Trizol reagent (Invitrogen), purified (RNeasy Protect Mini Kit, Qiagen) according to the manufacturer's instructions and stored at −80 °C. RNA purity was assessed and quantified by the 260/280 nm ratio in a Nanodrop device (ND-1000, NanoDrop Technologies, Thermo Fisher Scientific). RNA samples were treated with DNase (Sigma-Aldrich) and cDNAs were obtained by reverse-transcribe cDNA Synthesis kit (Thermo Scientific). cDNAs were amplified in triplicate in a rapid thermal cycler (LightCycler Instrument, Roche Diagnostics) with SYBR Green Master mix (Life Technologies) using 0.5 µM of each oligonucleotide. Primers were designed using the Primer Blast program (NCBI). Samples underwent 45 PCR cycles (2 min at 95 °C, 10 s at the melting temperature and 18 s at 72 °C). For each primer pair, the melting temperature was optimized. The primer pairs used in this study are shown in Table 1. Peptidylprolyl Isomerase A (*Ppia*) and phosphoglycerate kinase (*Pgk1*) housekeeping genes were used as an internal control for normalization. The relative quantification of the PCR products was done using the LightCycler 480 quantification software (Roche Molecular Biochemicals).

2.9. Lumbar spinal cords staining

Mice were anesthetized through intraperitoneal injection of a cocktail containing ketamine (90 mg/kg) and xylazine (10 mg/kg) in sterile normal saline and transcardially perfused with phosphate buffered saline (PBS) followed by 4% paraformaldehyde (PFA) in PBS. Isolated lumbar spinal cords were post-fixed in 4% PFA overnight at 4 °C and processed for frozen or paraffin techniques. The cryoprotection protocol consisted of a saccharose gradient (10%, 20% and 30%) performed before freezing. The tissues samples were placed in OCT embedding medium and frozen by liquid nitrogen. Frozen tissues were cut into 10 µm sections on a cryostat. On the other hand, paraffin-embedded tissue blocks were cut into 10 µm-transversal serial sections using a microtome. Paraffin tissues sections were pretreated for deparaffinization and rehydration before perfoming immunohistochemistry assays. Frozen and paraffin tissues sections were blocked in PBS, 5% normal goat serum, 4% BSA and 0.2% Triton X-100 for 2 h at RT and then, incubated with primary antibodies (prepared in PBS, 1% normal goat serum, 4% BSA and 0.2% Triton X-100) overnight at 4 °C. The next day, the slices were washed three times with PBS and incubated for 1 h with secondary antibodies at RT. Finally, after three rinses with PBS, the slices were counterstained with DAPI Fluoromont (Sigma-Aldrich).

2.10. Sciatic nerve staining

Mice were sacrificed by cervical dislocation and sciatic nerve were dissected and immediately frozen in liquid nitrogen and stored at −80 °C. They were placed in OCT embedding medium, frozen and cut into 7 µm sections on a cryostat. Nerves sections were fixed in PFA 4% for 7 min, blocked with 8% BSA and 1% Triton X-100 for 90 min at RT and then incubated with primary antibodies (prepared in PBS, 5% BSA and 0′1% triton X-100) overnight at 4 °C. The next day, the slices were washed with PBS-0′5% Tween-0′1% Triton and incubated for 3 h with secondary antibodies at RT. Finally, after several washes with PBS, the slices were mounted with Fluoromount-G with DAPI.

2.11. Antibodies

For negative controls, sections were incubated in parallel without primary antibody. The following primary antibodies were used: α-SMI-32 (1:1000, Covance), α-GFAP (1:700, Sigma-Aldrich), α-S100B (1:50, Abcam), α-IBA 1 (1:200, Wako), α-TUBB3 (1:700, Abcam), α-TUBB3 (1:500, Sigma-Aldrich), α-TUBB3 (1:500, Promega), α-pERK (1:50, Cell Signaling),α-TNF-α (1:100, Abcam), CD206 (1:40, R&D Systems), CD86 (1:100, BD Biosciences), α-SYNAPSIN-1 (1:75, Abcam) and α-PSD95 (1:150, Abcam). The secondary antibodies, diluted 1:500, were the

Table 1
RT-PCR oligonucleotides used to detect mRNAs in MNs.

Gene	Forward	Reverse
Tnfα	5′-AGCCCCCAGTCTGTATCCTT-3′	5′-GAGGCAACCTGACCACTCAACCG-3′
Cxc10	5′-CCAAGTGCTGCCGTCATTTTC-3′	5′-GGCTCGCAGGGATGATTTCAA-3′
C1qa	5′-TGTCCCACCATCAGCAAAGG-3′	5′-GTCTCCATGGTGTCCCTGC-3′
C1qb	5′-TCTAGGGACCCAGACTTCCG-3′	5′-AGGGGCTTCCTGTGTATGGA-3′
Gfap	5′-CGAAGAAAACCGCATCACCA-3′	5′-TTGAGGTGGCCTTCTGACAC-3′
S100b	5′-GACTCCAGCAGCAAAGGTGA-3′	5′-CTTCCTGCTCCTTGATTTCCTCCA-3′
MhcII	5′-CATTCAAGGCCTGCGATCAG-3′	5′-CTTGGTTTTGTGGGTCCTGG-3′
Itgam	5′-CATTCAAGGCCTGCGATCAG-3′	5′-CTTCCTGCTCCTTGATTTCCTCCA-3′
EphB2	5′-GCCGTGGAAGAAACCCTGAT-3′	5′-GTTCATGTTCTCGTCGTAGCC-3′
Synto	5′-CTGCATCCGTGGTCAACAG-3′	5′-GGGACTCCTATCCGCCATAC-3′
Pick1	5′-CTGGTGACGAGATCACTGGG-3′	5′-GACATGCCCTGCTTAGGGTC-3′
Chrm1	5′-ACCTCCCCTATCCACCTTCAG-3′	5′-AGAGTAAGGGCATCACCTTGG-3′
Htr2b	5′-TGGTCATCATGGCAGTGTCC-3′	5′-CCACCGGTACCCATACAGGA-3′
Ppia	5′-GCGTCTGCTTCGAGCTGTTTGC-3′	5′-CCAAAGACCACATGCTTGCCATCC-3′
Pgk1	5′-GGGTGTGAATCTGCCACAGAA-3′	5′-TTGCAGACAAGATCCAGCTGA-3′

following: donkey α-mouse Alexa Fluor 488, donkey α-rabbit Alexa Fluor 488, donkey α-mouse Alexa Fluor Texas Red, donkey α-rabbit Alexa Fluor 594, donkey α-mouse Alexa Fluor 594 and donkey α-goat Alexa Fluor 488 from Invitrogen, and donkey α-rat Alexa Fluor 488 from Abcam.

2.12. Images acquisition

Confocal images were acquired on a Leica TCS-SP8 X White Light Laser confocal microscope (Leica Microsystems) with Hybrid spectral detectors using a HC PL APO 20× and 40× oil immersion objectives (0.75 and 1.25 NA, respectively). The quantitative image analysis of the immunoreactivity was assessed using the Image J software (v1.37, National Institutes of Health).

2.13. Statistical analysis

All statistical analyses were performed using the GraphPad Prism 5.03 Software. The mean data were compared using an unpaired Student's two-tailed *t*-test to determine the significance of values between the experimental groups. The results were represented as means and standard error of the mean (SEM). Values of $P \leq 0.05$ were considered statistically significant.

3. Results

3.1. GDAP1 deficiency induces up-regulation of immune response pathways and oxidative stress

We investigated if GDAP1 deficiency induces neuroinflammation in mouse and if it was associated with oxidative stress in motor neurons (MNs). First, we studied how the lack of GDAP1 affects transcriptional pattern of immune response genes in mice spinal cord, where MNs somas are located. We identified 570 upregulated and 469 down-regulated genes at a *P* value threshold of 0.05 in the *Gdap1*$^{-/-}$ mice when compare to WT. Bioinformatic analysis using the Gene Ontology (GO) browser showed the significant upregulation in the *Gdap1*$^{-/-}$ mice of pathways related to innate and adaptive immune system (Fig. 1A). Specifically, we found the up-regulation of pathways related to protective immunity, inflammatory pathology and regulation of lymphocytes, and the significant down-regulation of regulatory pathways of immune-related processes (Fig. 1A). Then, we studied the presence of inflammation *in vivo* in the *Gdap1*$^{-/-}$ mice by detecting myeloperoxidase (MPO) activity of activated phagocytes using Xenolight Rediject inflammation probe (Fig. 1B). We observed the significant increase of average radiance in both total and maximum efficiency in the *Gdap1*$^{-/-}$ mice when compared to WT. This process was particularly localized in spinal cord and peritoneum. Overall, the transcriptome profile and the *in vivo* detection of MPO in the *Gdap1*$^{-/-}$ mice showed that the absence of GDAP1 is associated with the activation of inflammatory pathways.

As the lack of GDAP1 causes mitochondrial defects (Barneo-Munoz et al., 2015), we investigate whether inflammation associated with GDAP1 absence is related to redox homeostasis. We quantified the levels of cellular reactive oxygen species (ROS) and mitochondria superoxide in MNs primary cultures. We observed that *Gdap1*$^{-/-}$ MNs in comparison to WT showed both higher levels of ROS formation (Fig. 1C, left panel) and superoxide ion in mitochondria (Fig. 1C, right panel). In addition, *Gdap1*$^{-/-}$ MNs showed a significant increase of cell death and apoptotic cells with respect to WT neurons (Supplementary Fig. 1). Altogether these results showed that the absence of GDAP1 induces a higher oxidative status in neurons that probably activates the inflammatory response that we found in *Gdap1*$^{-/-}$ mice.

3.2. The *Gdap1*$^{-/-}$ mouse spinal cord and sciatic nerve show pro-inflammatory markers

To get a deeper insight into the impact of the inflammation pathology in *Gdap1*$^{-/-}$ mice spinal cord, we investigated the presence of gliosis performing immunofluorescence analysis of astrocytes and microglial cells. We used specifics antibodies to detect glial fibrillary acidic protein (GFAP) and S100 calcium-binding protein B (S100B), as astroglia-specific markers, and ionized calcium binding adapter molecule-1 (IBA1), as microglia and macrophages marker. In *Gdap1*$^{-/-}$ mice, we observed that GFAP-positive (+) cells presented hypertrophic cell body typical of reactive astrocytes (Fig. 2A, upper). Moreover, many of IBA1 labeled cells showed rounded cell bodies with shorted processes and amoeboid morphologies (Fig. 2A, lower), indicative of activated microglial cells. Immunofluorescence quantification showed a significant increase GFAP, S100B and IBA1 immunoreactivity in *Gdap1*$^{-/-}$ mice, compare to control mice (Fig. 2B). In addition, we found a significant upregulation of *Gfap*, *S100b*, *Mhc* class II and *Itgam* mRNA levels in the spinal cord of *Gdap1*$^{-/-}$ (Fig. 2C) but not in brain or cerebellum (Supplementary Fig. 2).

Next, we characterized the functional phenotypes of the innate immune response in *Gdap1*$^{-/-}$ mice by detecting anti-inflamatory (M2) and pro-inflamatory (M1) markers (Groh and Martini, 2017). Co-localization experiments using α-IBA1 with α-CD206 (Mannose Receptor C-Type 1, M2 marker) or α-CD86 (T-Lymphocyte Activation Antigen CD86, M1 marker) were performed in WT and *Gdap1*$^{-/-}$ mice spinal cords and sciatic nerve. We observed equal CD206 expression in WT and *Gdap1*$^{-/-}$ mice (Fig. 3A), which indicates that both genotypes exhibit anti-inflammatory features. In contrast, we found a significant increase of the pro-inflammatory M1 marker CD86 signal in both the spinal cord ($P < 0.001$) and the sciatic nerve ($P < 0.001$) in *Gdap1*$^{-/-}$ mice (Fig. 3B). In addition, axonal damage was assessed by staining the unphosphorylated neurofilament heavy chain SMI-32. We found high SMI-32 signal in *Gdap1*$^{-/-}$ mice that was not present in WT mice (Supplementary Fig. 3), confirming axonal damage associated with lack of GDAP1.

3.3. Absence of GDAP1 induces expression of inflammatory mediators

To investigate the activation of the innate immunity and the generation of inflammatory mediators in the *Gdap1*$^{-/-}$ mice, we studied the expression of inflammatory markers in sciatic nerve and spinal cord as CMT target tissues. Total protein from 5- and 12-month old mice were studied (Fig. 4A and B). Western blot experiments revealed significant differences in the *Gdap1*$^{-/-}$ mice in comparison to WT. Tumor necrosis factor alpha (TNF-α), a cytokine involve in systemic inflammation, showed a significant increase in both sciatic nerve (Fig. 4A) and lumbar spinal cord (Fig. 4B) at both ages. Phosphorylated extracellular signal–regulated kinases (pERK), which controls TNF-α secretion in glia cells and neurons during inflammatory response (Coquenlorge et al., 2014; Mir et al., 2008), was increased in sciatic nerve from 5 month-old and in spinal cord at 12 month-old mice (Fig. 4A and B). Conversely, cJun NH2-terminal kinases (JNK) signaling pathway, which is also involved in *Tnfα* regulation (Ventura et al., 2003), showed no differences (Fig. 4A and B). The Interferon Regulatory Factor 3 (IRF3) was increased exclusively in spinal cord at both ages (Fig. 4B). These changes were not observed in brain and cerebellum (Supplementary Fig. 4).

To further evaluate the inflammatory response status in the *Gdap1*$^{-/-}$ mice spinal cord, we performed RT-PCR of *Tnfα*, C-X-C motif chemokine ligand 10 gene (*Cxcl10*), complement C1q A chain (*C1qa)* and complement C1q B chain (*C1qb*) genes (Fig. 4C). We found a significant upregulation for all these genes in the *Gdap1*$^{-/-}$ mice, thus supporting activation of innate immune response in spinal cord.

To define the cell types involved in the activation of inflammatory response in *Gdap1*$^{-/-}$ mice spinal cord, we performed double

immunostaining of neural-specific markers with p-ERK1/2 or TNF-α (mediators elevated in both sciatic nerve and spinal cord). *Gdap1*$^{-/-}$ mice showed a pERK expression increment mostly in neurons (TUBB3 + cells) and microglia (IBA1 + cells), but also in some astrocytes (S100 + cells) (Fig. 5A). TNF-α expression was only detected in *Gdap1*$^{-/-}$ mice. Specifically, TNF-α was mostly expressed in microglia cells and to lesser

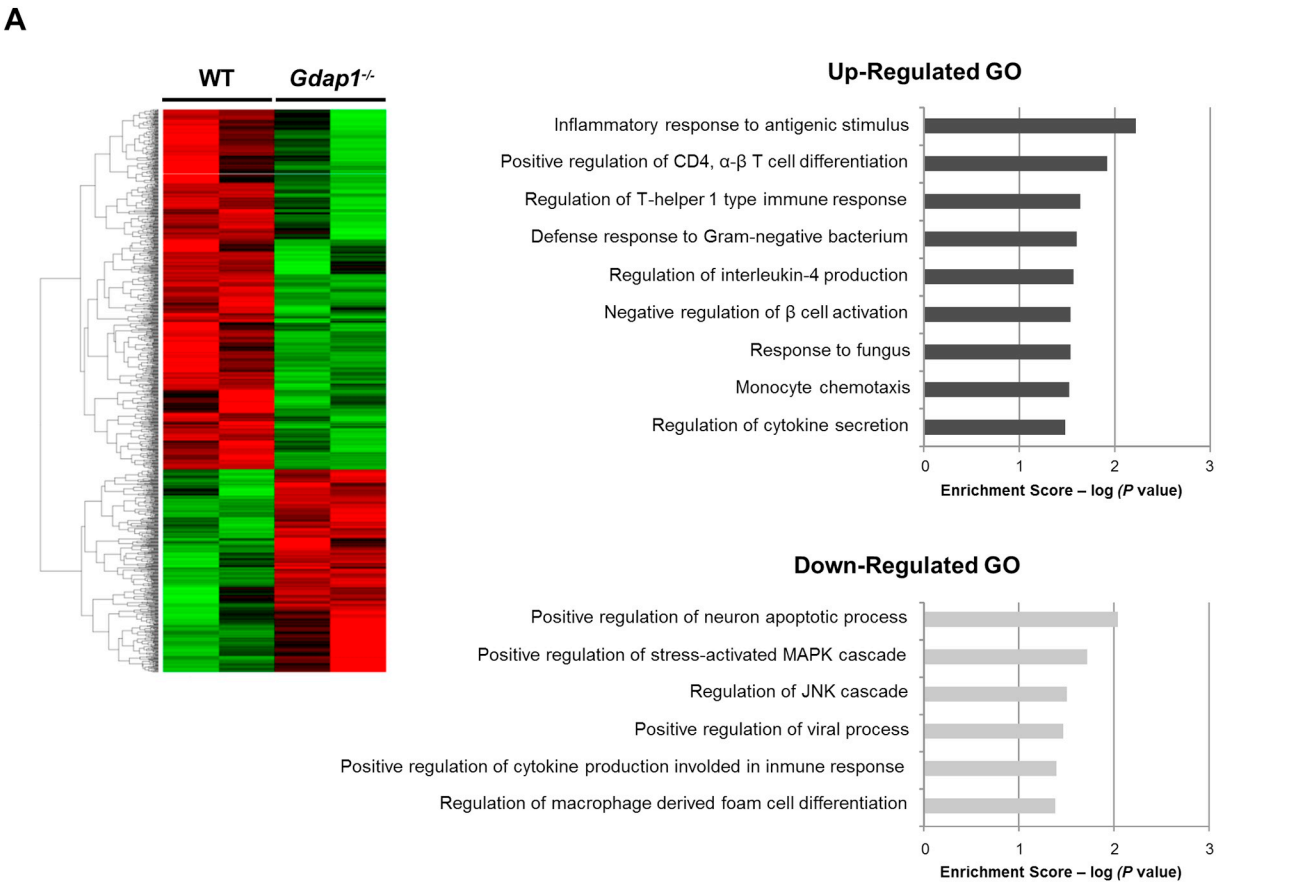

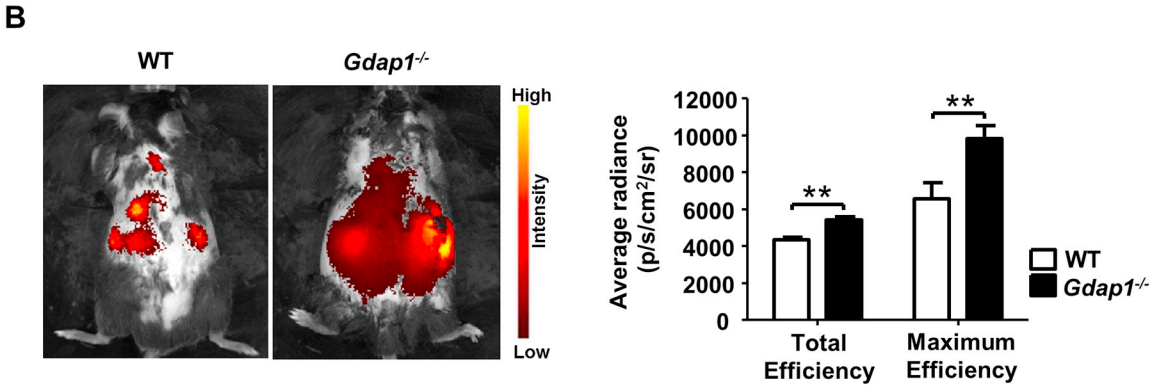

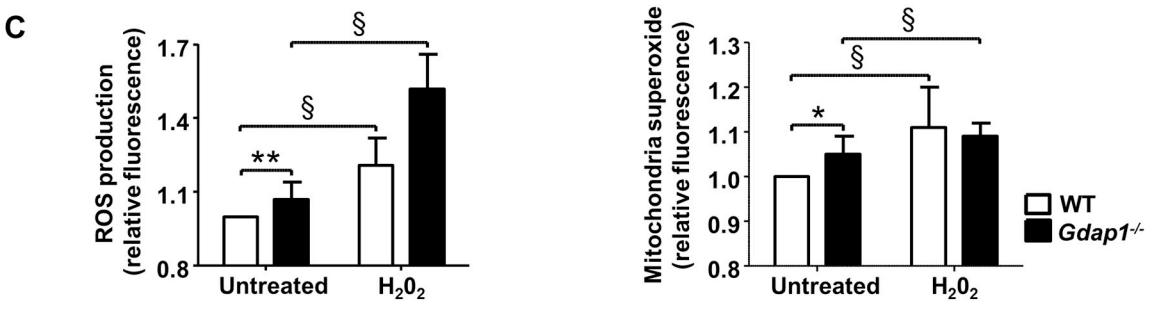

(caption on next page)

Fig. 1. The lack of GADP1 causes an upregulation of immune system pathways and an increase of oxidative stress in MNs primary cultures.
A) Heatmap of normalized data representing color-coded expression levels of differentially expressed genes in *Gdap1*$^{-/-}$ spinal cord mice compare to WT mice. Positive log-ratios (log fold change) are shown in red, while negative log-ratios are shown in green. Gene ontology (GO) terms for up- and downregulated pathways in the *Gdap1*$^{-/-}$ mice were represented (right panel). *P*-values determined by Fisher's exact test are expressed as the negative logarithm (base 10). B) *In vivo* bioluminescent imaging of WT and *Gdap1*$^{-/-}$ mice after 24 h injection of Xenolight Rediject Inflammation Probe. The optical signal was quantified from the ROIs drawn manually and expressed as the average radiance in photon/s/ cm^2/sr (p/s/cm2/sr). Data are means ± SEM from 3 independent experiments. $^{**}P < 0.01$. **C)** DCFH-DA or MitosSOX staining were used to detect ROS production and mitochondrial superoxide, respectively, in MNs primary cultures. MNs were treated with hydrogen peroxide to induce oxidative stress. Data are means + SEM from 6 independent experiments. $^{*}P < 0.05$, $^{**}P < 0.01$ for comparison between untreated *Gdap1−/− versus* (*vs*) WT MNs and, § $P < 0.05$ for comparison between treated *vs* untreated MNs. (For interpretation of the references to color in this figure legend, the reader is referred to the web version of this article.)

extent in some astrocytes (S100+ cells) and in a few neurons (TUBB3+ cells) (Fig. 5B).

3.4. The loss of GDAP1 alters synaptic homeostasis in spinal cord

Since neuroinflammation potentially contributes to synapse loss (Mottahedin et al., 2017), we evaluate the expression of genes and proteins related to synaptic organization and function in spinal cord. We quantified by RT-PCR the Ephrin type-B receptor 2 (*Ephb2*) gene, which is involved in neuronal plasticity (Grunwald et al., 2001), two postsynaptic markers genes (Synaptopodin [Synpo]) and protein interacting with PRKCA1 [Pick1]), and two receptor genes (cholinergic receptor muscarinic 1 [Chmr1] and 5-hydroxytryptamine receptor 2B [Htr2b]). We found all markers increased in the *Gdap1*$^{-/-}$ mice (Fig. 6A). In addition, Western blot analysis showed that the *Gdap1*$^{-/-}$ mice had an increase of SYNAPSIN-1, a phosphoprotein of synaptic vesicles that modulates the neurotransmitter release (Cesca et al., 2010), while the postsynaptic density protein 95 (PSD95) did not show any changes (Fig. 6B). We also performed double immunolabeling with α -TUBB3 and either α -PSD95 or α -SYNAPSIN-1 (Fig. 6C). While quantification of total signal intensity showed no differences (Fig. 6D, left panel), a significant decrease was found in the area labeled with either PSD95 or SYNAPSIN-1 (Fig. 6D, right panel). These results suggest dysfunctional changes in *Gdap1−/−* mice synapsis at spinal cord.

4. Discussion

The role of innate and adaptive immune response and inflammation in genetic peripheral neuropathies is not fully understood. In this study, we present evidence that neuroinflammation could play a pathophysiological role of the neuropathy associated *Gdap1*-null mouse, as a model of *GDAP1*-related recessive CMT axonopathy.

Our findings in *Gdap1*$^{-/-}$ mice and cultured MNs can be summarized as follows: first, the GO analysis of transcriptome data from spinal cord showed deregulation of several immune responses pathways; second, the *in vivo* detection of higher levels of phagocytes activation in the spinal cord; third, the presence of pro-inflammatory markers in the spinal cord and sciatic nerve; and fourth, the significant increase of inflammatory proteins of innate immune system in spinal cord and sciatic nerve.

A number of evidences have shown the role of innate immune response in the pathophysiology of peripheral axonopathies. Studies in animal models have shown complement-mediated disruption of node of Ranvier channels, which in turn disrupts ionic homeostasis (Susuki et al., 2007) and contributes to axonal damage. In this way, treatment with anti-C1q monoclonal antibodies attenuated activation of complement cascade and deposition as well as it reduced the recruitment of immune cells and axonal injury (McGonigal et al., 2016). In the case of demyelinating CMT, animal models for different causative genes show that inflammation is a common pathogenic feature (Martini and Willison, 2016). For instance, a CMT1X model shows secondary inflammation involving detrimental macrophage activation that intensifies demyelination, Schwann cell dedifferentiation and axons dysfunction (Groh et al., 2015). By contrast, nerve crush injury induces macrophages activation to clear debris and regulates Schwann cell function during nerve regeneration (Stratton et al., 2018).

In the *Gdap1*$^{-/-}$ mice, a model for primary axonal CMT, we observed an increase of inflammatory response in both spinal cord and sciatic nerve associated with axonal damage, which may participate in the pathophysiology that we have previously observed in this model (Barneo-Munoz et al., 2015). GDAP1 is located at MOM and mutations in *GDAP1* gene produce mitochondrial alterations. It is known that dysfunctional mitochondria generate high levels of ROS that could activate the redox-sensitive inflammatory pathway and the inflammasome. Both of these pathways promote the production of inflammatory cytokines leading to an overstimulation of the inflammatory response (Lopez-Armada et al., 2013). On the other hand, ROS production by dysfunctional mitochondria can also induce neuronal damage. As a consequence, neurons release various range of damage-associated molecular patterns (DAMPS), which are molecules recognized by the innate immune system and able to develop an inflammatory response (Krysko et al., 2011). In the present work, we detected excess of ROS and mitochondrial superoxide in the *Gdap1*$^{-/-}$ MNs thus suggesting that mitochondrial dysfunction might be responsible for triggering the inflammatory response.

The finding of mRNA upregulation of glial markers and reactive gliosis in the spinal cord of *Gdap1*$^{-/-}$ mice indicated a relevant inflammatory process in the spinal cord that can extend to the sciatic nerve or *viceversa*, but not in the brain and cerebellum. Several studies in animal models of neurodegenerative diseases have demonstrated different microglia phenotypes along disease stage, neuroprotective or neurotoxic in early or late phases, respectively (Kobayashi et al., 2013; Liao et al., 2012; Tang and Le, 2016). We found expression of both M2 neuroprotective and M1 neurotoxic microglia and macrophage markers in *Gdap1*$^{-/-}$ mice spinal cord and sciatic nerve, respectively. Microglia and macrophage activation may lead to the release of inflammatory mediators and neurotoxic molecules amplifying inflammatory response and ongoing neuronal damage (Block et al., 2007). Indeed, *Gdap1*$^{-/-}$ mice also showed increase of inflammatory mediators of the innate immune response in spinal cord and sciatic nerve. pERK increase was found in MNs, astrocytes and microglia cells in spinal cord of *Gdap1*$^{-/-}$ mice. It is known that neuronal oxidative stress activates ERK signaling pathway that plays a detrimental role in neurons promoting neuronal cell death (Satoh et al., 2000). On the other hand, activation of ERK signaling also controls the regulation of inflammatory cytokine and ROS production in astrocytes and microglia during inflammatory response (Ben Haim et al., 2015; Qian et al., 2007; Zhao et al., 2011). In others CMT models, the activation of ERK signaling pathway has also been associated with neuroinflammation and neurodegeneration. Specifically, ERK signaling activation upregulates Schwann cell-borne monocyte chemoattractant protein-1 (MCP-1) causing axon damage and demyelination in CMT1 models (Kohl et al., 2010). Moreover, the *in vivo* inhibition of the MEK-ERK pathway in CMT1X mice diminishes macrophage elevation and demyelination (Groh et al., 2010).

TNF-α, it is a pro-inflamamatory cytokine that plays an important role in the propagation of inflammation due to the activation and recruitment of immune cells (Bradley, 2008). Although glial cells are the major source of TNF-α (Chung and Benveniste, 1990; Hanisch, 2002; Welser-Alves and Milner, 2013), neurons are also able to produce TNF-α during neuroinflammation (Janelsins et al., 2008; Kiaei et al., 2006; Yoshihara et al.,

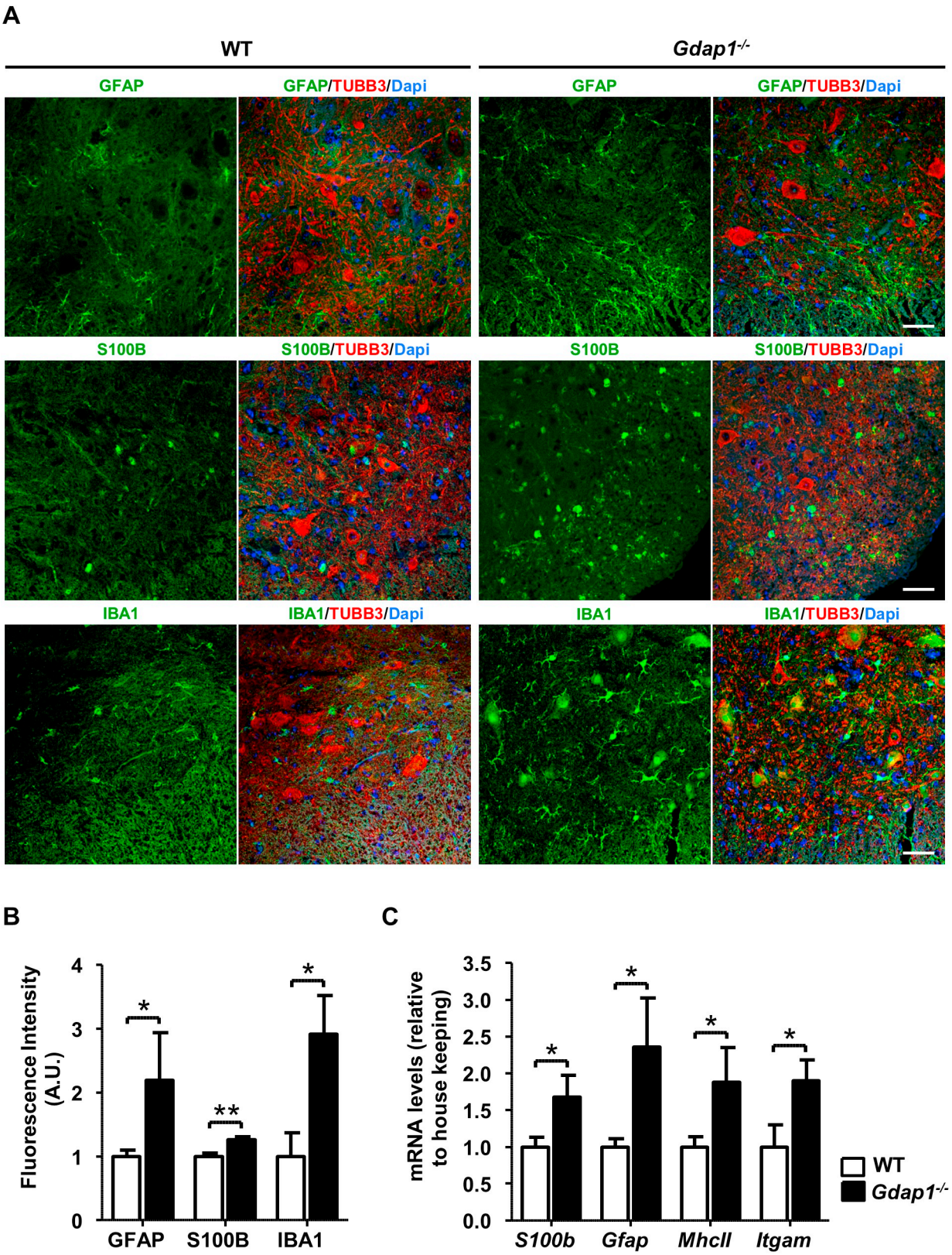

Fig. 2. *Gdap1*$^{-/-}$ mice show reactive gliosis in spinal cord.
A) Inmunostaining of astrocyte (GFAP and S100B), microglia (IBA1) and neuronal (TUBB3) markers in spinal cord transverse sections of WT (left) and *Gdap1*$^{-/-}$ (right) mice. Images were taken from confocal optical sections that are representative for the group averages. Arrows indicate hypertrophic astrocytes and activated microglia. Scale bar: 50 μm. B) Quantification of fluorescence intensity (A.U., arbitrary units) from 3 independent samples using Image J 1.37v. Data represent mean ± SEM. **C)** RT-PCR analysis of the astroglial activation markers Gfap and S100b and the microglia activation markers Mhc II and Itgam genes from WT and *Gdap1*$^{-/-}$ mice in spinal cord. Data are means ± SEM from 6 independent experiments. $^{*}P < 0.05$, $^{**}P < 0.01$.

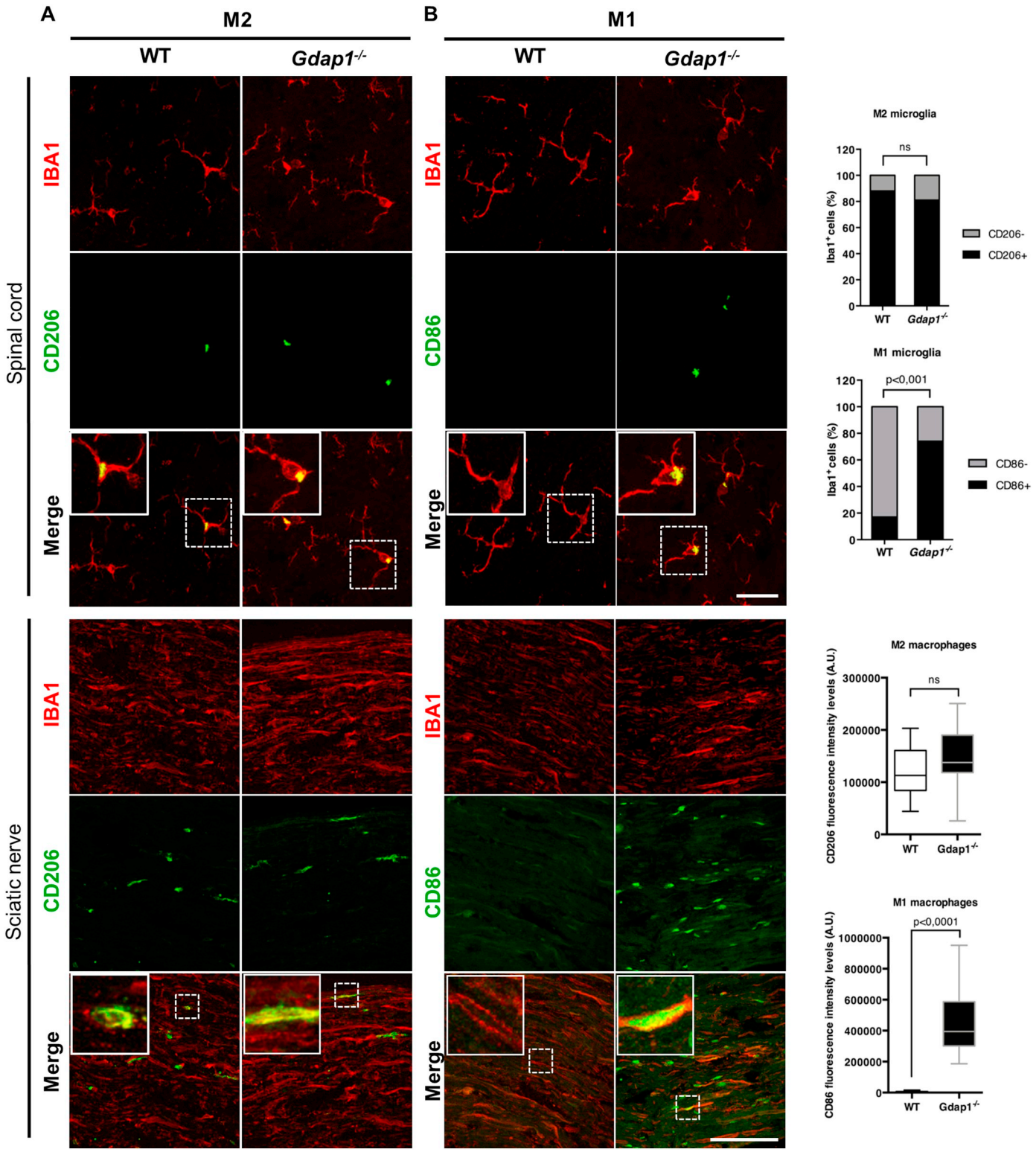

Fig. 3. Immunofluorescence visualization of M2 and M1 microglia and macrophage markers in spinal cord and sciatic nerve of WT and *Gdap1*$^{-/-}$ mice. WT and *Gdap1*$^{-/-}$ mice spinal cords and sciatic nerve were stained with α-IBA1 (microglia/macrophage marker) and either α-CD206 (M2 marker) or α-CD86 (M1 marker). A) CD206 expression was detected in microglia cells from WT and *Gdap1*$^{-/-}$ mice. B) High expression of CD86 was observed in microglia and macrophages of *Gdap1*$^{-/-}$ mice. Scales bar: 30 μm (spinal cord) and 100 μm (sciatic nerve). Quantification of IBA1 positive (+) cells (percentage) with CD206 (IBA1+ cells WT = 43, KO = 49) or CD86 (IBA1+ cells WT = 53, KO = 38) are shown in the right site of spinal cord panels. Quantification of CD206 or CD86 fluorescence intensity levels (A.U.) are shown in the right site of sciatic nerve panel. Data are median and interquartile rage (n = 10 images (60 mm^2 each) from 2 sciatic nerves of each genotype).

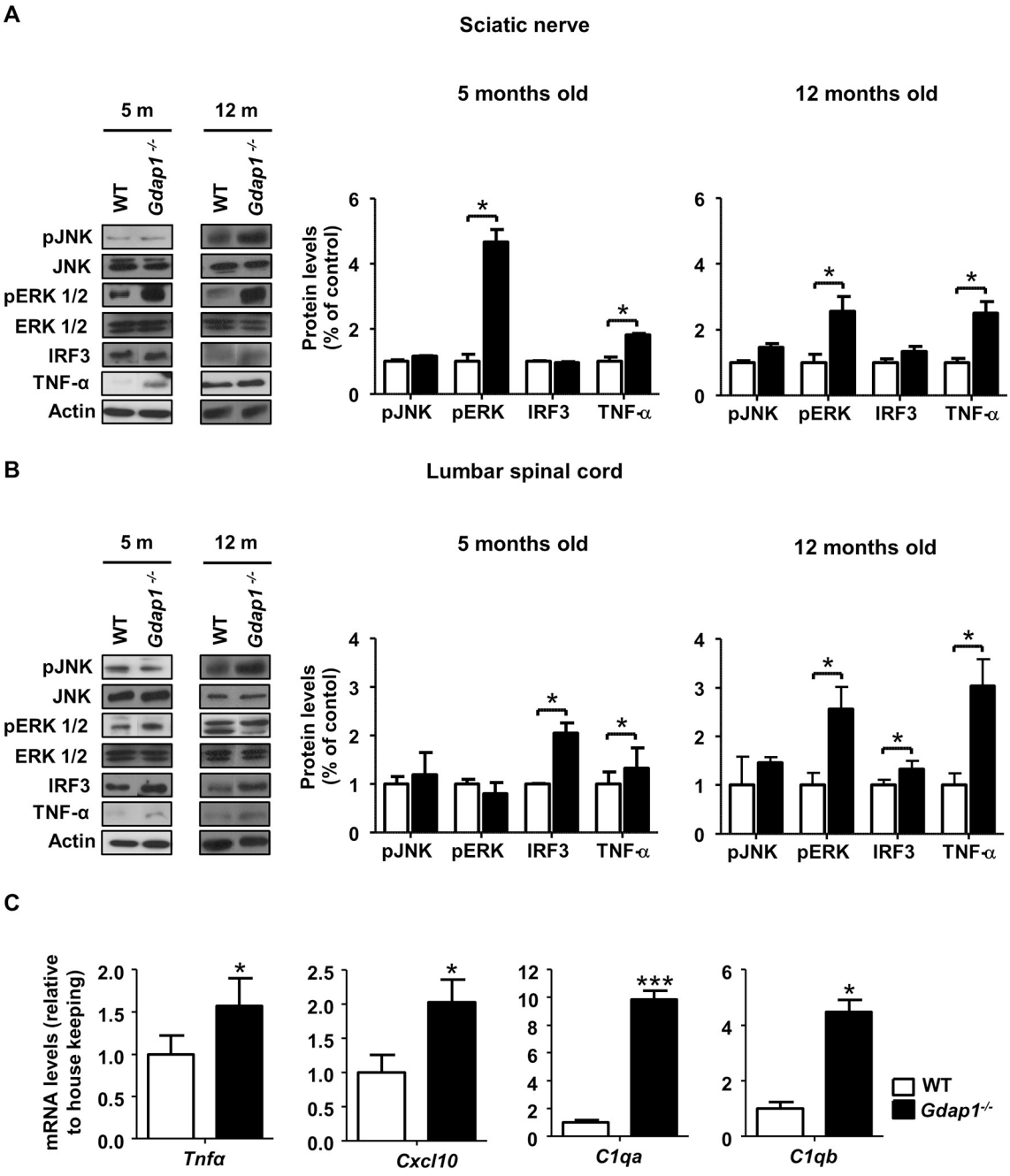

Fig. 4. GDAP1 deficiency promotes an inflammatory process in spinal cord and sciatic nerve.
Western blot and quantification of pERK, pJNK, IRF3 and TNF-α in sciatic nerve (A) and spinal cord (B) from 5- and 12-month-old mice. Relative protein expression of western blot bands was quantified using Image J 1.37v. Data are means ± SEM from 5 independent experiments. **C)** RT-PCR analysis of Tnfα, IP10 and C1qa and C1qb genes in spinal cord samples from WT and *Gdap1*$^{-/-}$ mice. Data are means ± SEM from 8 independent experiments. $^{*}P < 0.05$, $^{***}P < 0.001$.

2002). We found that mostly microglia, but also some astrocytes expressed high levels of TNF-α in spinal cord *Gdap1*$^{-/-}$ mice. Moreover, we also observed an increase of TNF-α expression in a few MNs of spinal cord, which might implicate neuron-glial interactions during the inflammatory process of neurodegeneration. It has been reported that antibodies against TNF-α prevented the loss of myelinated and unmyelinated fibers in a mouse model of a neuropathy (Ale et al., 2014). Furthermore, in CMT1A patients, melatonin treatment reduces the hyperoxidative and inflammatory condition normalizing pro-inflammatory cytokines including TNF-α (Chahbouni et al., 2017). Thus, the upregulation of *Tnfα* expression and ERK signaling in the axonal neuropathy of the *Gdap1*$^{-/-}$ mice allows proposing common treatment approaches for genetic CMT neuropathies, either axonal or demyelinating.

Finally, we observed in the *Gdap1*$^{-/-}$ spinal cord an increase of mRNA for proteins involved in neuronal plasticity and the decrease in the area labeled with synaptic markers in MNs. Neuroinflammation have been directly linked to synaptic dysfunction in many neurodegenerative disorders. Many studies suggest that microglia cells are responsible for synapse elimination through activation of classical complement pathway (Mottahedin et al., 2017; Stephan et al., 2012). Interestingly, we found a

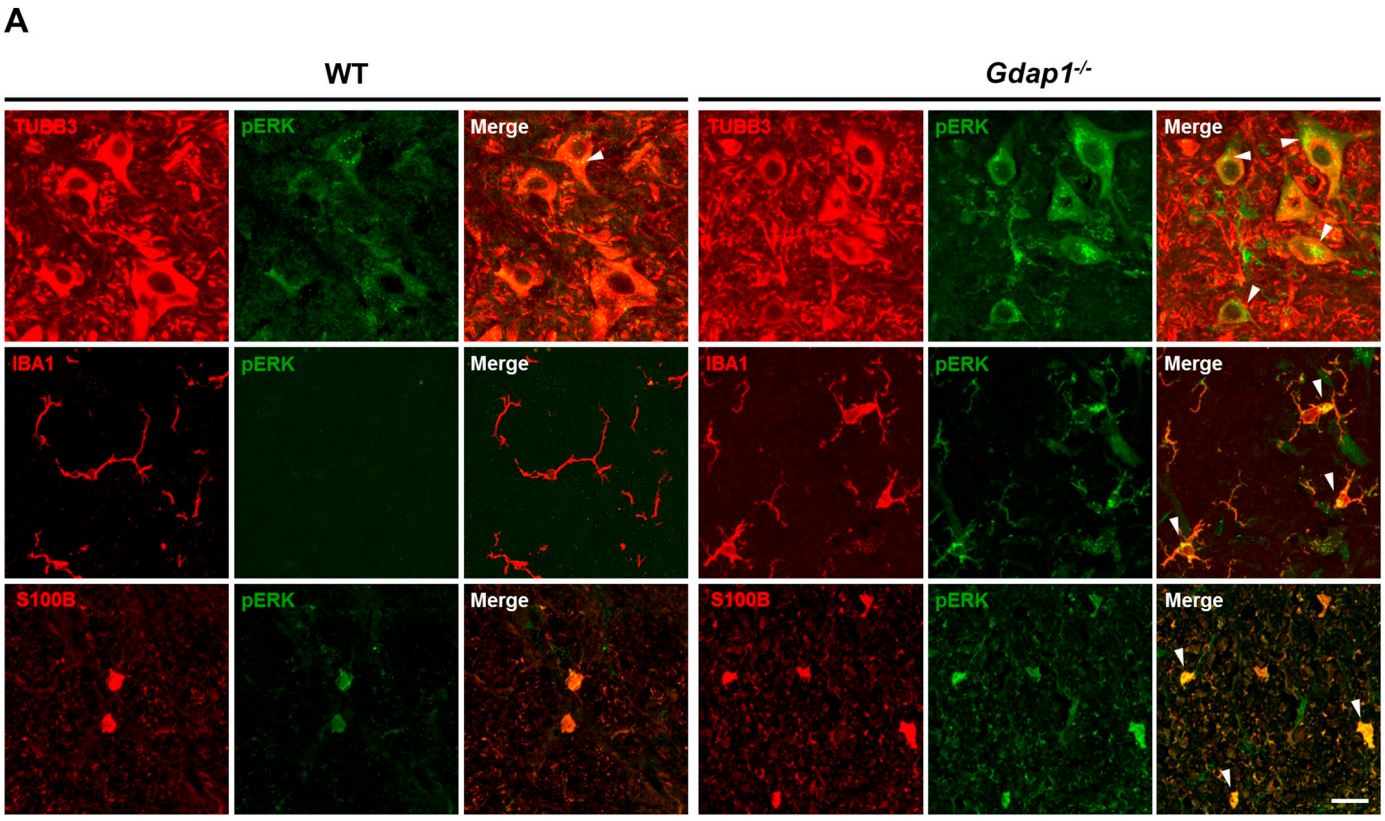

(caption on next page)

Fig. 5. Characterization of pERK and TNF-α inmmunoreactivity cells in spinal cord.
Double labeling immunofluorescence of pERK (A) and TNF-α (B) with TUBB3 (neuronal marker), IBA1 (microglia marker) or S100B (astrocyte marker) in spinal cord sections of WT and *Gdap1*$^{-/-}$ mice. A) Intense pERK immunoreactivity was observed mostly in neurons (TUBB3) and microglia (IBA1), and in a subset of astrocytes (S100B) in *Gdap1*$^{-/-}$ mice, compare to control mice. B) Co-localization of TNF-α was not detected with either neuronal or glial markers in WT mice. In contrast, TNF-α was co-localized predominantly with microglia (IBA1) in *Gdap1*$^{-/-}$ mice. It was also colocalized with some astrocytes (S100B) and minimally with a few neurons (TUBB3).
Scale bar: 20 μm. Arrow heads indicate the co-localized cells.

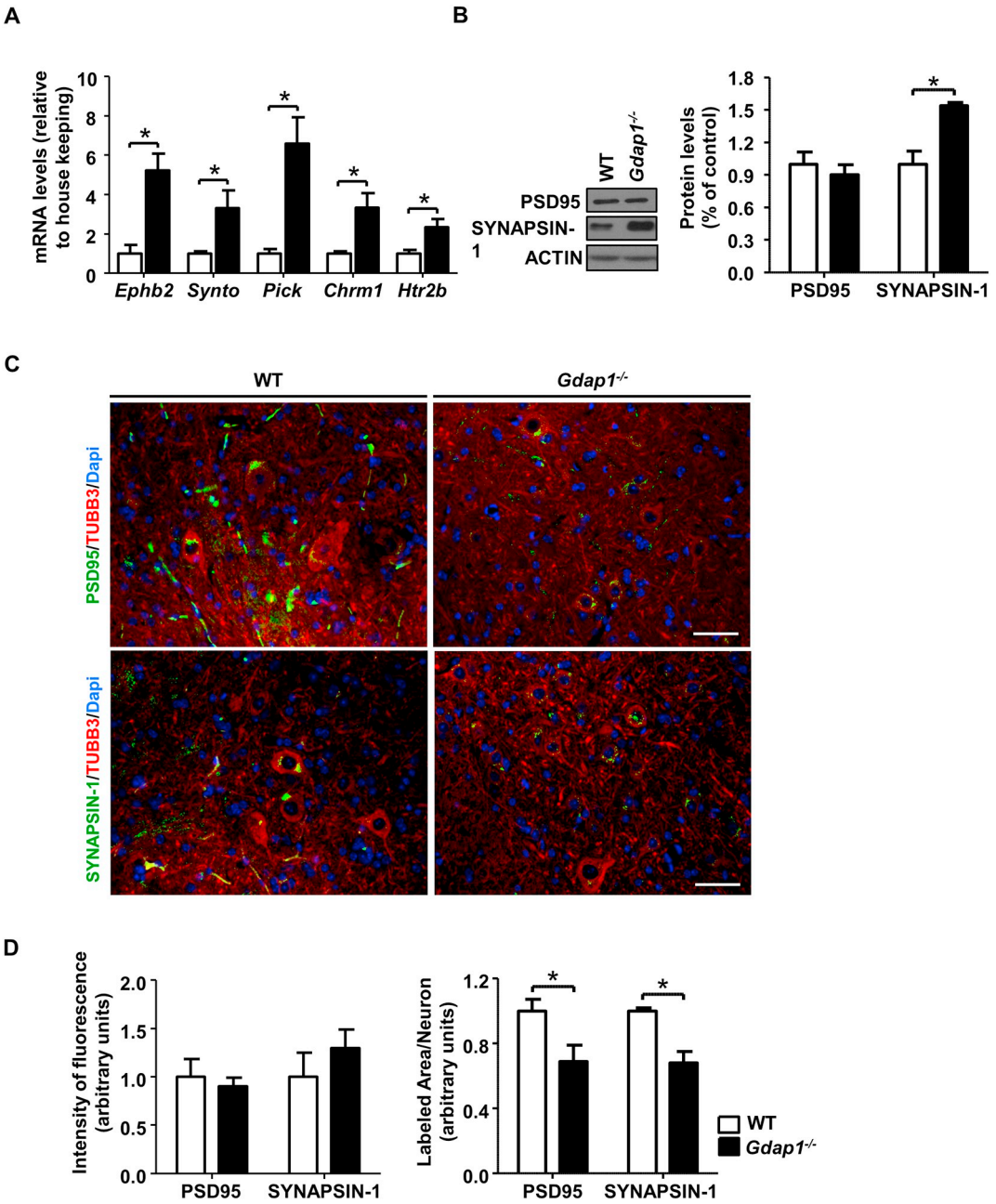

Fig. 6. GDAP1 deficiency cause changes in spinal cord synaptic homeostasis. RT-PCR analysis of Ephb2, Synto, Pick1, Chmr1 and Htr2b genes (A) and immunoblot of PSD95 and SYNAPSIN-1 (B), in spinal cord samples of WT and *Gdap1*$^{-/-}$ mice. Data are means ± SEM from 5 independent experiments. C) Inmunostaining of synaptic markers PSD95 and SYNAPSIN-1, and TUBB3 as neurons marker in spinal cord of WT and *Gdap1*$^{-/-}$ mice. Images were taken from confocal optical sections that are representative for the group averages. Scale bar: 50 μm. **D)** Quantification of fluorescence intensity (a.u.) from 4 independent samples was performed using Image J 1.37v. $^{*}P < 0.05$.

significant upregulation of *C1qa* and *C1qb* complement system genes in the spinal cord of *Gdap1*$^{-/-}$. Therefore, we postulate that the abnormal physiology at synapses in the *Gdap1*$^{-/-}$ spinal cord could be related not only to the axonopathy itself but also to the associated neuroinflammation and reactive gliosis (Chung et al., 2015).

5. Conclusions

We have demonstrated that inflammation in spinal cord and sciatic nerve, but not in brain and cerebellum, is part of the pathophysiology in a mouse model of axonal *GDAP1*-related CMT. These findings may open

new approaches for the treatment of the disease, with specificity in the axon recovering.

Supplementary data to this article can be found online at https://doi.org/10.1016/j.expneurol.2019.113004.

Funding

This work has been supported by the Spanish Ministry of Science, Innovation and Universities [grant no. SAF2015-66625-R], the Collaborative Joint Project awarded by IRDiRC and funded by the Instituto de Salud Carlos III (ISCIII) [grant no. IR11/TREAT-CMT], the Generalitat Valenciana Programme PROMETEOII [grant no. 2014/029], and the Generalitat de Catalunya [grant no. 2015 FEDER/S-21]. This work has also been funded by the CIBERER and CIBERSAM, which are initiatives from the ISCIII. The Department of Genetic and Molecular Medicine, Hospital Sant Joan de Déu, is part of the 'Centre Daniel Bravo de Diagnòstic i Recerca en Malalties Minoritàries'.

Declarations of interest

None

References

Ale, A., Bruna, J., Morell, M., van de Velde, H., Monbaliu, J., Navarro, X., Udina, E., 2014. Treatment with anti-TNF alpha protects against the neuropathy induced by the proteasome inhibitor bortezomib in a mouse model. Exp. Neurol. 253, 165–173.

Barneo-Munoz, M., Juarez, P., Civera-Tregon, A., Yndriago, L., Pla-Martin, D., Zenker, J., Cuevas-Martin, C., Estela, A., Sanchez-Arago, M., Forteza-Vila, J., Cuezva, J.M., Chrast, R., Palau, F., 2015. Lack of GDAP1 induces neuronal calcium and mitochondrial defects in a knockout mouse model of charcot-marie-tooth neuropathy. PLoS Genet. 11, e1005115.

Baxter, R.V., Ben Othmane, K., Rochelle, J.M., Stajich, J.E., Hulette, C., Dew-Knight, S., Hentati, F., Ben Hamida, M., Bel, S., Stenger, J.E., Gilbert, J.R., Pericak-Vance, M.A., Vance, J.M., 2002. Ganglioside-induced differentiation-associated protein-1 is mutant in Charcot-Marie-tooth disease type 4A/8q21. Nat. Genet. 30, 21–22.

Ben Haim, L., Carrillo-de Sauvage, M.A., Ceyzeriat, K., Escartin, C., 2015. Elusive roles for reactive astrocytes in neurodegenerative diseases. Front Cell Neurosci 9, 278.

Block, M.L., Zecca, L., Hong, J.S., 2007. Microglia-mediated neurotoxicity: uncovering the molecular mechanisms. Nat. Rev. Neurosci. 8, 57–69.

Bradley, J.R., 2008. TNF-mediated inflammatory disease. J Pathol. 214, 149–160.

Cesca, F., Baldelli, P., Valtorta, F., Benfenati, F., 2010. The synapsins: key actors of synapse function and plasticity. Prog. Neurobiol. 91, 313–348.

Chahbouni, M., Lopez, M.D.S., Molina-Carballo, A., de Haro, T., Munoz-Hoyos, A., Fernandez-Ortiz, M., Guerra-Librero, A., Acuna-Castroviejo, D., 2017. Melatonin treatment reduces oxidative damage and normalizes plasma pro-inflammatory cytokines in patients suffering from Charcot-Marie-Toth neuropathy: A Pilot Study in Three Children. Molecules 22.

Chung, I.Y., Benveniste, E.N., 1990. Tumor necrosis factor-alpha production by astrocytes. Induction by lipopolysaccharide, IFN-gamma, and IL-1 beta. J. Immunol. 144, 2999–3007.

Chung, W.S., Welsh, C.A., Barres, B.A., Stevens, B., 2015. Do glia drive synaptic and cognitive impairment in disease? Nat. Neurosci. 18, 1539–1545.

Claramunt, R., Pedrola, L., Sevilla, T., Lopez de Munain, A., Berciano, J., Cuesta, A., Sanchez-Navarro, B., Millan, J.M., Saifi, G.M., Lupski, J.R., Vilchez, J.J., Espinos, C., Palau, F., 2005. Genetics of Charcot-Marie-Tooth disease type 4A: mutations, inheritance, phenotypic variability, and founder effect. J. Med. Genet. 42, 358–365.

Coquenlorge, S., Duchalais, E., Chevalier, J., Cossais, F., Rolli-Derkinderen, M., Neunlist, M., 2014. Modulation of lipopolysaccharide-induced neuronal response by activation of the enteric nervous system. J. Neuroinflammation 11, 202.

Cuesta, A., Pedrola, L., Sevilla, T., Garcia-Planells, J., Chumillas, M.J., Mayordomo, F., LeGuern, E., Marin, I., Vilchez, J.J., Palau, F., 2002. The gene encoding ganglioside-induced differentiation-associated protein 1 is mutated in axonal Charcot-Marie-Tooth type 4A disease. Nat. Genet. 30, 22–25.

Di Filippo, M., Chiasserini, D., Tozzi, A., Picconi, B., Calabresi, P., 2010. Mitochondria and the link between neuroinflammation and neurodegeneration. J. Alzheimers Dis. 20 (Suppl. 2), S369–S379.

Gingras, M., Gagnon, V., Minotti, S., Durham, H.D., Berthod, F., 2007. Optimized protocols for isolation of primary motor neurons, astrocytes and microglia from embryonic mouse spinal cord. J. Neurosci. Methods 163, 111–118.

Gonzalez-Sanchez, P., Pla-Martin, D., Martinez-Valero, P., Rueda, C.B., Calpena, E., Del Arco, A., Palau, F., Satrustegui, J., 2017. CMT-linked loss-of-function mutations in GDAP1 impair store-operated Ca(2+) entry-stimulated respiration. Sci. Rep. 7, 42993.

Groh, J., Martini, R., 2017. Neuroinflammation as modifier of genetically caused neurological disorders of the central nervous system: understanding pathogenesis and chances for treatment. Glia 65, 1407–1422.

Groh, J., Heinl, K., Kohl, B., Wessig, C., Greeske, J., Fischer, S., Martini, R., 2010. Attenuation of MCP-1/CCL2 expression ameliorates neuropathy in a mouse model for Charcot-Marie-Tooth 1X. Hum. Mol. Genet. 19, 3530–3543.

Groh, J., Klein, I., Hollmann, C., Wettmarshausen, J., Klein, D., Martini, R., 2015. CSF-1-activated macrophages are target-directed and essential mediators of Schwann cell dedifferentiation and dysfunction in Cx32-deficient mice. Glia 63, 977–986.

Grunwald, I.C., Korte, M., Wolfer, D., Wilkinson, G.A., Unsicker, K., Lipp, H.P., Bonhoeffer, T., Klein, R., 2001. Kinase-independent requirement of EphB2 receptors in hippocampal synaptic plasticity. Neuron 32, 1027–1040.

Hanisch, U.K., 2002. Microglia as a source and target of cytokines. Glia 40, 140–155.

Janelsins, M.C., Mastrangelo, M.A., Park, K.M., Sudol, K.L., Narrow, W.C., Oddo, S., LaFerla, F.M., Callahan, L.M., Federoff, H.J., Bowers, W.J., 2008. Chronic neuron-specific tumor necrosis factor-alpha expression enhances the local inflammatory environment ultimately leading to neuronal death in 3xTg-AD mice. Am. J. Pathol. 173, 1768–1782.

Jerath, A., Ferguson, N.D., Steel, A., Wijeysundera, D., Macdonald, J., Wasowicz, M., 2015. The use of volatile anesthetic agents for long-term critical care sedation (VALTS): study protocol for a pilot randomized controlled trial. Trials 16, 560.

Kiaei, M., Petri, S., Kipiani, K., Gardian, G., Choi, D.K., Chen, J., Calingasan, N.Y., Schafer, P., Muller, G.W., Stewart, C., Hensley, K., Beal, M.F., 2006. Thalidomide and lenalidomide extend survival in a transgenic mouse model of amyotrophic lateral sclerosis. J. Neurosci. 26, 2467–2473.

Kobayashi, K., Imagama, S., Ohgomori, T., Hirano, K., Uchimura, K., Sakamoto, K., Hirakawa, A., Takeuchi, H., Suzumura, A., Ishiguro, N., Kadomatsu, K., 2013. Minocycline selectively inhibits M1 polarization of microglia. Cell Death Dis. 4, e525.

Kohl, B., Fischer, S., Groh, J., Wessig, C., Martini, R., 2010. MCP-1/CCL2 modifies axon properties in a PMP22-overexpressing mouse model for Charcot-Marie-tooth 1A neuropathy. Am. J. Pathol. 176, 1390–1399.

Krysko, D.V., Agostinis, P., Krysko, O., Garg, A.D., Bachert, C., Lambrecht, B.N., Vandenabeele, P., 2011. Emerging role of damage-associated molecular patterns derived from mitochondria in inflammation. Trends Immunol. 32, 157–164.

Liao, B., Zhao, W., Beers, D.R., Henkel, J.S., Appel, S.H., 2012. Transformation from a neuroprotective to a neurotoxic microglial phenotype in a mouse model of ALS. Exp. Neurol. 237, 147–152.

Lopez-Armada, M.J., Riveiro-Naveira, R.R., Vaamonde-Garcia, C., Valcarcel-Ares, M.N., 2013. Mitochondrial dysfunction and the inflammatory response. Mitochondrion 13, 106–118.

Martínez-Valero, P., 2017. Enfermedad de Charcot-Marie-Tooth asociada a Gdap1: alteraciones en nocicepción y señalización por calcio. PhD Thesis. Autonomous University of Madrid, Cantoblanco, Madrid. Teseo: Doctoral Theses Database, Spanish Ministry of Education.

Martini, R., Willison, H., 2016. Neuroinflammation in the peripheral nerve: cause, modulator, or bystander in peripheral neuropathies? Glia 64, 475–486.

McGonigal, R., Cunningham, M.E., Yao, D., Barrie, J.A., Sankaranarayanan, S., Fewou, S.N., Furukawa, K., Yednock, T.A., Willison, H.J., 2016. C1q-targeted inhibition of the classical complement pathway prevents injury in a novel mouse model of acute motor axonal neuropathy. Acta Neuropathol. Commun. 4, 23.

Mir, M., Tolosa, L., Asensio, V.J., Llado, J., Olmos, G., 2008. Complementary roles of tumor necrosis factor alpha and interferon gamma in inducible microglial nitric oxide generation. J. Neuroimmunol. 204, 101–109.

Mottahedin, A., Ardalan, M., Chumak, T., Riebe, I., Ek, J., Mallard, C., 2017. Effect of Neuroinflammation on synaptic organization and function in the developing brain: implications for neurodevelopmental and neurodegenerative disorders. Front. Cell. Neurosci. 11, 190.

Niemann, A., Ruegg, M., La Padula, V., Schenone, A., Suter, U., 2005. Ganglioside-induced differentiation associated protein 1 is a regulator of the mitochondrial network: new implications for Charcot-Marie-Tooth disease. J. Cell Biol. 170, 1067–1078.

Noack, R., Frede, S., Albrecht, P., Henke, N., Pfeiffer, A., Knoll, K., Dehmel, T., Meyer Zu Horste, G., Stettner, M., Kieseier, B.C., Summer, H., Golz, S., Kochanski, A., Wiedau-Pazos, M., Arnold, S., Lewerenz, J., Methner, A., 2011. Charcot-Marie-Tooth disease CMT4A: GDAP1 increases cellular glutathione and the mitochondrial membrane potential. Hum. Mol. Genet. 21, 150–162.

Pedrola, L., Espert, A., Wu, X., Claramunt, R., Shy, M.E., Palau, F., 2005. GDAP1, the protein causing Charcot-Marie-Tooth disease type 4A, is expressed in neurons and is associated with mitochondria. Hum. Mol. Genet. 14, 1087–1094.

Pla-Martin, D., Rueda, C.B., Estela, A., Sanchez-Piris, M., Gonzalez-Sanchez, P., Traba, J., de la Fuente, S., Scorrano, L., Renau-Piqueras, J., Alvarez, J., Satrustegui, J., Palau, F., 2013. Silencing of the Charcot-Marie-Tooth disease-associated gene GDAP1 induces abnormal mitochondrial distribution and affects Ca2+ homeostasis by reducing store-operated Ca2+ entry. Neurobiol. Dis. 55, 140–151.

Qian, L., Tan, K.S., Wei, S.J., Wu, H.M., Xu, Z., Wilson, B., Lu, R.B., Hong, J.S., Flood, P.M., 2007. Microglia-mediated neurotoxicity is inhibited by morphine through an opioid receptor-independent reduction of NADPH oxidase activity. J. Immunol. 179, 1198–1209.

Qin, L., Liu, Y., Wang, T., Wei, S.J., Block, M.L., Wilson, B., Liu, B., Hong, J.S., 2004. NADPH oxidase mediates lipopolysaccharide-induced neurotoxicity and proinflammatory gene expression in activated microglia. J. Biol. Chem. 279, 1415–1421.

Rossor, A.M., Lu, C.H., Petzold, A., Malaspina, A., Laura, M., Greensmith, L., Reilly, M.M., 2016. Plasma neurofilament heavy chain is not a useful biomarker in Charcot-Marie-Tooth disease. Muscle Nerve 53, 972–975.

Satoh, T., Nakatsuka, D., Watanabe, Y., Nagata, I., Kikuchi, H., Namura, S., 2000. Neuroprotection by MAPK/ERK kinase inhibition with U0126 against oxidative stress in a mouse neuronal cell line and rat primary cultured cortical neurons. Neurosci. Lett. 288, 163–166.

Soler, R.M., Egea, J., Mintenig, G.M., Sanz-Rodriguez, C., Iglesias, M., Comella, J.X., 1998. Calmodulin is involved in membrane depolarization-mediated survival of 26

motoneurons by phosphatidylinositol-3 kinase- and MAPK-independent pathways. J. Neurosci. 18, 1230–1239.
Stephan, A.H., Barres, B.A., Stevens, B., 2012. The complement system: an unexpected role in synaptic pruning during development and disease. Annu. Rev. Neurosci. 35, 369–389.
Stratton, J.A., Holmes, A., Rosin, N.L., Sinha, S., Vohra, M., Burma, N.E., Trang, T., Midha, R., Biernaskie, J., 2018. Macrophages regulate Schwann cell maturation after nerve injury. Cell Rep. 24, 2561–2572 e2566.
Susuki, K., Rasband, M.N., Tohyama, K., Koibuchi, K., Okamoto, S., Funakoshi, K., Hirata, K., Baba, H., Yuki, N., 2007. Anti-GM1 antibodies cause complement-mediated disruption of sodium channel clusters in peripheral motor nerve fibers. J. Neurosci. 27, 3956–3967.
Tang, Y., Le, W., 2016. Differential roles of M1 and M2 microglia in neurodegenerative diseases. Mol. Neurobiol. 53, 1181–1194.
Ventura, J.J., Kennedy, N.J., Lamb, J.A., Flavell, R.A., Davis, R.J., 2003. c-Jun NH(2)-terminal kinase is essential for the regulation of AP-1 by tumor necrosis factor. Mol. Cell. Biol. 23, 2871–2882.
Welser-Alves, J.V., Milner, R., 2013. Microglia are the major source of TNF-alpha and TGF-beta1 in postnatal glial cultures; regulation by cytokines, lipopolysaccharide, and vitronectin. Neurochem. Int. 63, 47–53.
Yoshihara, T., Ishigaki, S., Yamamoto, M., Liang, Y., Niwa, J., Takeuchi, H., Doyu, M., Sobue, G., 2002. Differential expression of inflammation- and apoptosis-related genes in spinal cords of a mutant SOD1 transgenic mouse model of familial amyotrophic lateral sclerosis. J. Neurochem. 80, 158–167.
Zhao, S., Zhang, L., Lian, G., Wang, X., Zhang, H., Yao, X., Yang, J., Wu, C., 2011. Sildenafil attenuates LPS-induced pro-inflammatory responses through down-regulation of intracellular ROS-related MAPK/NF-kappaB signaling pathways in N9 microglia. Int. Immunopharmacol. 11, 468–474.